Composites Science and Technology 168 (2018) 126–132

Contents lists available at ScienceDirect

Composites Science and Technology

journal homepage: www.elsevier.com/locate/compscitech

A highly stretchable carbon nanotubes/thermoplastic polyurethane fiber-shaped strain sensor with porous structure for human motion monitoring

Xiaozheng Wang, Hongling Sun, Xiaoyan Yue, Yunfei Yu, Guoqiang Zheng, Kun Dai*, Chuntai Liu, Changyu Shen

School of Materials Science and Engineering, The Key Laboratory of Advanced Materials Processing & Mold of Ministry of Education, Zhengzhou University, Zhengzhou, 450001, China

ARTICLE INFO

Keywords:
A: Flexible composites
A: Carbon nanotubes
A: Polymer-matrix composites (PMCs)
B: Electrical properties

ABSTRACT

Highly flexible and stretchable strain sensors play an important role in the wearable electronic systems. Up to now, it is still an enormous challenge to achieve a good balance between the wide response range and high sensitivity for a resistive-type flexible strain sensor. In this work, we prepared a fiber-shaped strain sensor based on thermoplastic polyurethane (TPU) and multi-walled carbon nanotubes (MWCNTs) via a simple and cost-efficient wet-spun method. The production process can satisfy continuous and large-scale preparation. The generation of the interesting porous structure is related to the solvent exchange in solidification process and beneficial to the improvement of the sensing range. In the uniaxial stretching test, the MWCNTs/TPU fiber-shaped sensor showed an ultra-wide workable strain range (320%), a high sensitivity (gage factor of 22.2 within 160% strain and 97.1 for strain of 160–320%) and a fast response time (< 200 ms). The MWCNTs/TPU composite fiber sensor exhibited good reproducibility and excellent durability in multi-cycle test (9700 cycles at 100% strain). The mechanism of the response behavior was studied through the tunneling theory. The strain sensor shows potential applications in human motion detections including bending of the fingers, elbows and knee, squatting and squat-jumping. The present paper provides an effective strategy for the design of high performance fiber-shaped wearable electronic systems.

1. Introduction

Strain sensors with flexible, stretchable, and wearable features have attracted great attentions for their applications in health monitoring [1–3], joint movement [4–8], wearable electronics [9] and robotics [10], etc. For a favorable strain sensor, good flexibility, high sensitivity, wide response range and excellent durability are always required simultaneously. Conductive polymer composites (CPCs), with the advantage of excellent flexibility, low-cost, good processability and workability, have been widely concerned as the candidates for strain sensing materials [11,12]. For the CPCs based strain sensor, metal fillers (such as Ag nanoparticles, Ag nanosheets, gold nanowires) and carbonaceous fillers (such as carbon nanotubes (CNTs), carbon black (CB) and graphene) are two types of frequently-used conductive materials [4,13–15]. Nevertheless, metal fillers exhibit many defects: poor acid and alkali-tolerance, high cost and inferior ability for surface modification, which limit their applications in human motion monitoring [16]. Compared to the metal fillers, carbonaceous fillers with excellent electrical properties and good flexibility (like CNT or graphene) are more sensible choices in the preparation of CPCs [17,18].

CPC based strain sensors have achieved rapid development recently [19–21], nevertheless, there are still many problems needed to be resolved, for example, the conflict between wide response range and high sensitivity, complex production process and large-scale production, etc [4,5]. Zhi et al. reported a core-shell yarn strain sensor, which is produced by winding native cotton yarns around urethane continuous filament plus coating the CNTs onto the surface of the yarns [22]. The sensor shows a large stretchability (300%), while its sensitivity is low (GF = 2.15 at 25% strain), and the technology needs to perform multiple preparation steps. Lu et al. adopt the layer-by-layer CB assembly technique to prepare a fiber-shaped wearable strain sensor [12]. The fabrication approach is simple and cost-efficient. The strain sensor possesses a high sensitivity (GF = 70.6 below 1% strain), while it could hardly demand the detection of large strain. Huang et al. obtained a thermoplastic polyurethane (TPU)@CNT@polypyrrole (PPy) (TCP) fiber via drawing CNT array on a fixed TPU fiber and electrodepositing PPy onto the TPU@CNT fiber [23]. The preparation process is complicated, time-consuming and toxic to some extent, and it is difficult to

* Corresponding author.
E-mail address: kundai@zzu.edu.cn (K. Dai).

https://doi.org/10.1016/j.compscitech.2018.09.006
Received 27 July 2018; Received in revised form 3 September 2018; Accepted 8 September 2018
Available online 13 September 2018
0266-3538/ © 2018 Elsevier Ltd. All rights reserved.

achieve a large-scale preparation. Considering the sensitivity and response range, the TCP fibers show a relatively low sensitivity (GF of 10.8 at 65% strain) and a narrow response range (below 65% strain). Although a great deal of efforts have been made to improve the sensitivity, increase the response range and receive a large-scale production, few of them have achieved a nice balance between the three key points.

In this work, to achieve a practical strain sensor with a wide response range, high sensitivity and large-scale preparation, we fabricated a strain sensor based on TPU and multi-walled carbon nanotubes (MWCNTs). TPU was selected as the matrix due to its excellent flexibility and plasticity [24,25]. MWCNTs was utilized as conductive fillers owing to their outstanding electrical properties, superior mechanical properties, ready availability and large aspect ratio [26]. The composite fibers were fabricated using a simple and cost-efficient wet-spun method, which could easily enable a large-scale preparation. To study the strain sensing behaviors of the composite fibers, uniaxial tensile tests and multi-cycle response tests were conducted, respectively. The mechanism of the response behavior was studied via a mathematic model. The capability of the composite fiber on human motions was demonstrated by monitoring the bending of the fingers, elbows and knee, squatting and squat-jumping. The results indicate that our preparation strategy provides a good candidate to achieve a high performance flexible strain sensor for human motion monitoring.

2. Experimental

2.1. Materials

The MWCNTs (Model TNIM2 with diameter of about 8–15 nm, length of 30–50 μm, specific surface area of and 250–300 m^2/g and the true density of about 2.1 g/cm^3) and corresponding CNTs dispersant (TNDDIS) were provided by Chengdu Organic Chemicals Co. Ltd., Chinese Academy of Science. MWCNTs were dried at 120 °C in vacuum for 3 h before usage. Polyester-based thermoplastic polyurethane (TPU) (Elastollan 1185A) was purchased from BASF Co. Ltd. Dimethylformamide (DMF) was supplied by Fuyu Fine Chemical Co., Ltd, Tianjin, China and used as received without further treatment.

2.2. The fabrication of composite fibers

The MWCNTs/TPU composite fibers were fabricated by a wet-spun technique (Fig. 1a). For the details, (1) MWCNTs and the dispersant with the mass ratio of 5:1 were added into 25 ml DMF and treated under ultrasonication (KQ-600DE, Kunshan Ultrasonic instrument Co. Ltd, China) for 15 min to enable the MWCNTs to be dispersed homogenously. (2) 5 g TPU was put into the suspension under magnetic stirring (85–2, Jintan Zhongda Instrument Factory, China) for 5 h at room temperature to obtain a homogeneous mixture. (3) The mixture was then treated by ultrasonication for another 2 h and stirred for 10 min. (4) The resulting mixture was drawn into a 10 mL syringe and then extruded through a single axis needle into coagulation bath, which was filled with deionized (DI) water and the temperature was maintained at 25 °C. The as-spun composite fibers was placed in the DI water for 20 min to form a stable fiber, and then dried in air. The obtained composite fiber possesses a high stretchability and excellent flexibility (Fig. 1b and c). As shown in Fig. 1d and e, composite fibers with the length of 4 m could be received and wound on a cylinder or placed in a petri dish, exhibiting the trait of large-scale production. Fig. 1f shows that a cassock knot woven by our composite fiber can stand on a flower without bending the petals, indicating a good weavability and the lightweight feature.

2.3. Preparation of strain sensor

As shown in Fig. S1, the MWCNTs/TPU composite fibers were cut to 5 cm for testing. The copper tapes were mounted on two ends of fibers as electrodes. In order to guarantee the good contact, silver paste was employed to connect the tiny gap between samples and the electrodes.

2.4. Characterization

Field emission scanning electron microscope (FE-SEM, Model JEOL JSM-7500F) was utilized to characterize the morphology and microstructure of MWCNTs/TPU fibers. To observe the inner pore diameter and MWCNTs distribution of the composite fibers, the samples were immersed into liquid nitrogen for 1 h and then cryo-fractured. The Optical microscope images of MWCNTs/TPU composite fibers were obtained by using a digital microscope (Leica DVM6, United States Leica Microsystems Inc.). The resistance of the MWCNTs/TPU composite fibers was measured by a digit precision multimeter (DM4050, Tektronix). The electric current signal and response time were obtained by an electrochemical workstation (RST5200, Suzhou Resitest Electronic Co., Ltd., China).

For the electromechanical analyses, an electronic tensile testing machine with a 100 N load cell (UTM2203, Shenzhen Suns Technology Stock Co. Ltd, China) coupled with the multimeter were employed to record electrical signals synchronously under various stretching modes. MWCNTs/TPU strain sensors were attached onto different joints via the aid of medical waterproof polyurethane (PU) membranes to assess the sensing ability. The electrical signals resulting from the joints' motions were recorded on-line by using the RST5200 electrochemical workstation.

3. Results and discussion

3.1. Morphology

The morphology of pure TPU fiber and the MWCNTs/TPU composite fiber were observed and compared by using the SEM firstly. In Fig. 2a, a hollow structure of the pure TPU fiber is observed clearly and there were many small pores on the cell walls (Fig. 2b). The fascinating internal structure of the composite fibers might be caused by the differences between mass transfer rate of the inward layer and outward layer [27,28]. Another reason is possibly related to the exchange process between the DMF solvent and DI water (the coagulating bath). The DI water occupied a certain volume inside the MWCNTs/TPU composite fibers in the solidification process [29], and it was then evaporated during the post-processing, leading to the interesting porous structure. In the enlarged cross section of the pure TPU fiber, no conductive fillers could be observed on the cell walls (Fig. 2c).

Fig. 2d shows the cross section of a MWCNTs/TPU composite fiber. It is observed that the porous structure instead of the obvious hollow structure is displayed in the cross section, which is attributed to inhibition of solvent exchange due to the addition of conductive fillers [29]. From the enlarged view (Fig. 2e), it can be seen that most of the holes are blind holes. The aperture size of the pure TPU fibers and composite fibers were counted in Figs. S2 and 3, respectively. Due to the presence of the porous structure, conductive fillers-MWCNTs were selectively distributed in the cell walls [30,31], they were observed in SEM micrographs (Fig. 2f). The SEM micrograph of the surface morphology of pure TPU fibers and MWCNTs/TPU composite fibers are shown in Fig. S4, respectively. It can be seen from the magnified SEM images of the pure TPU fiber and composite fiber (Figs. S4b and d) that there are no obvious defects on the surfaces. The surface and cross section morphology of MWCNTs/TPU composite fibers with different diameter are shown in Figs. S5 and S6, respectively.

3.2. Electromechanical properties

When the loading is applied on a resistive-type strain sensor, the electrical resistance will be changed, which is mainly attributed to the evolution of conductive network [32,33]. The electrical responsivity is

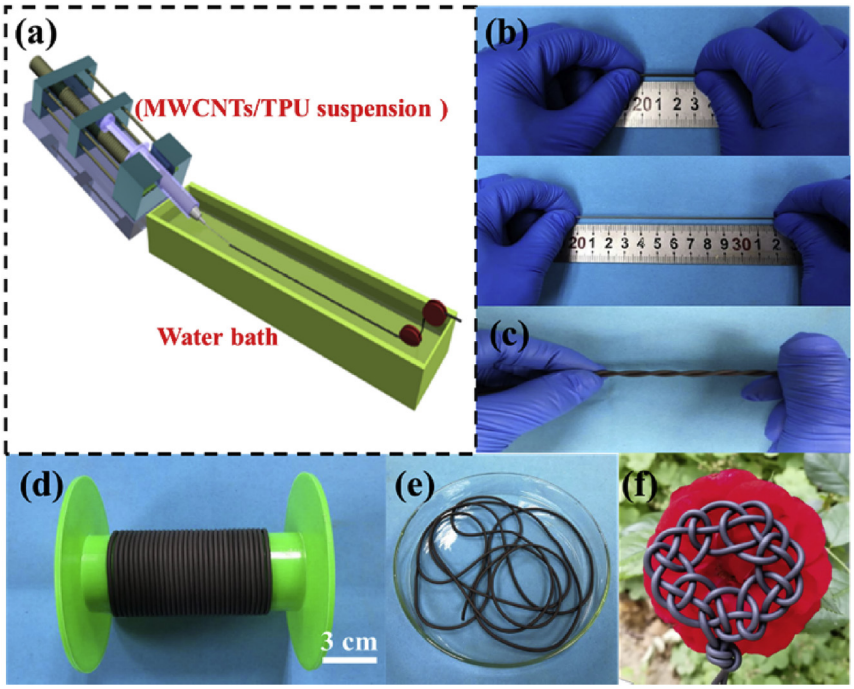

Fig. 1. MWCNTs/TPU composite fibers. a) Schemes of the process for the preparation of MWCNTs/TPU composite fibers by wet spinning method. The exhibition of flexible features of MWCNTs/TPU composite fibers under (b) stretching, and (c) twisting. d, e) The as-spun fiber wrapped around a cylinder over 4 m or placed on a petri dishes. f) A cassock knot woven by MWCNTs/TPU composite fiber on a flower.

generally defined by the electrical resistance variation ratios, $(\Delta R/R_0 = (R_t - R_0)/R_0)$ where R_t represents the electrical resistance at a certain strain and R_0 is the original resistance. The GF is also used to explain the sensitivity of the strain sensor, which is evaluated by the equation: $GF = \frac{\Delta R / R_0}{\varepsilon}$, where ε represents the applied strain.

Fig. 3a shows the stress-strain and $\Delta R/R_0$-strain curves for the fiber-shaped MWCNTs/TPU composite strain sensor with a stretching speed of 10 mm/min. For the mechanical property, the stress rises gradually with the increasing of the strain. For the strain sensing behavior, the $\Delta R/R_0$ of the strain sensor increases exponentially as the strain increases. It is attractive that the strain sensor can always have the electrical response before breakage, which exhibits the wide response range. As shown in Fig. 3b, the $\Delta R/R_0$-strain curve could be divided into two linear areas with various slopes, generating two GFs. The GF is 22.1 for strain range within 160% and 97.5 for strain of 160–320%, proving the elasticity and high sensitivity of the strain sensor. Interestingly, the strain sensor have good linearity ($R^2 > 0.985$) within 30% strain (the inset in Fig. 3b). Although there are many reports about flexible strain sensor based on CPCs, they rarely achieve a balance between the response range and sensitivity. Nevertheless, a strain > 50% for human motion detection is necessary. A high sensitivity is also essential for detecting human motions. Compared with the other reported strain sensors based on elastomers [12,23], the fabricated fiber-shaped strain sensor with porous structure displays a wider response range and high GF. The detailed comparison is clearly shown in Fig. 3c. The strain sensing performances of composite fibers with different diameter are shown in Fig. S7.

The current-voltage feature of the strain sensor with different tensile strains is shown in Fig. 4a. A good linear relationship between the current and voltage is observed from the plot under different strain loadings, demonstrating that the strain sensor obey the Ohm's law. Besides, the resistance increases monotonically with the increasing of tensile strain, which further proves the electricity response behavior under applied strain [19]. Fig. 4b depicts the response time of the strain sensor. The response time is < 200 ms and measured via applying a tensile loading (5% strain) with a high rate (500 mm/min). Then we measured the $\Delta R/R_0$ response of MWCNTs/TPU strain sensor at 20–200 mm/min under 150% strain (Fig. S8). It is observed that the

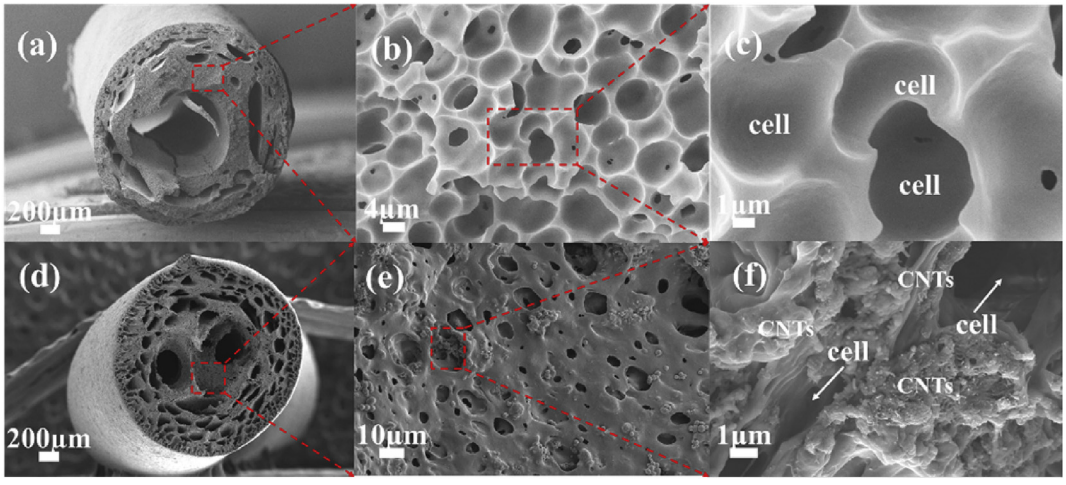

Fig. 2. SEM photographs of the cross section of pure TPU fibers (a–c) and MWCNTs/TPU composite fibers (d–e) with different magnifications.

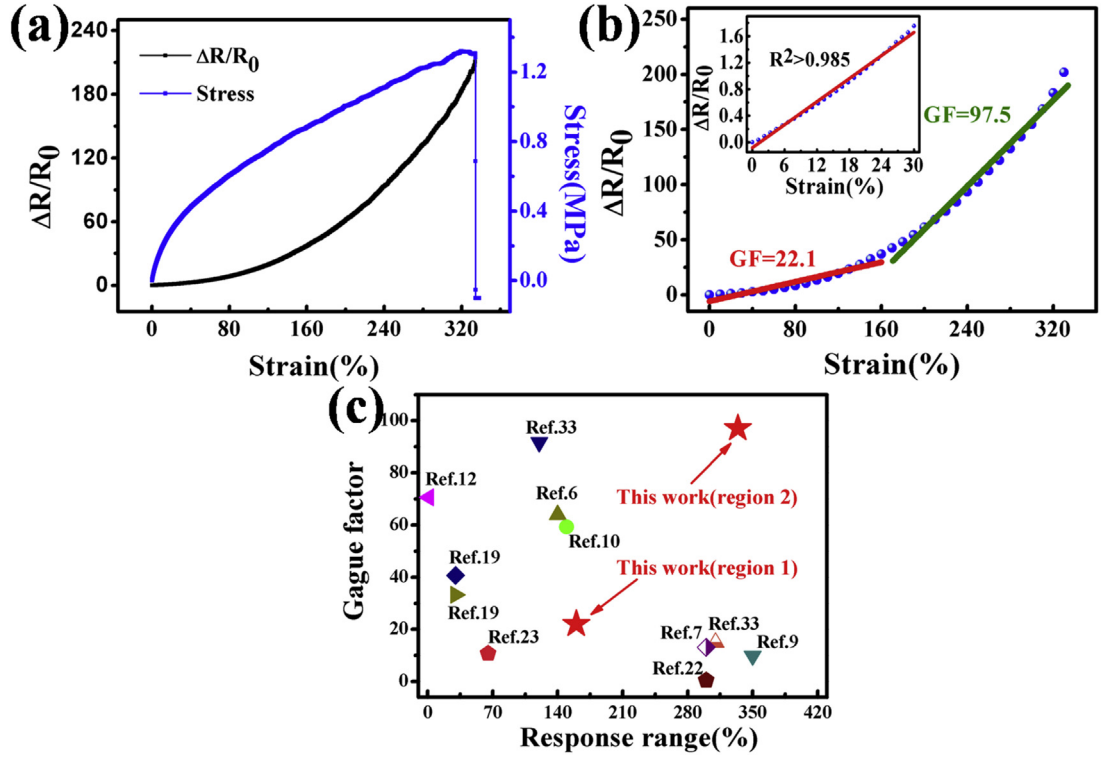

Fig. 3. (a) Typical stress-strain and $\Delta R/R_0$-strain curves for MWCNTs/TPU composite strain sensor. (b) Relative change in resistance of the MWCNTs/TPU composite strain sensor towards applied strain. (c) Comparison of the GF and maximum working range of MWCNTs/TPU composite strain sensor with the recent reports.

higher tensile speed do not deteriorate the performance of the MWCNTs/TPU strain sensor, indicating the good recoverability and stability in electrical signals.

To better evaluate the strain sensing behavior of the fabricated strain sensor during the cyclic extension, the strain sensor is then measured in uniaxial cyclic stretching. Fig. 4c shows that our strain sensor possesses a stable electrical signal when it is applied 60, 120, 180, 240, and 300% strain during 20 stretching-releasing cycles. The

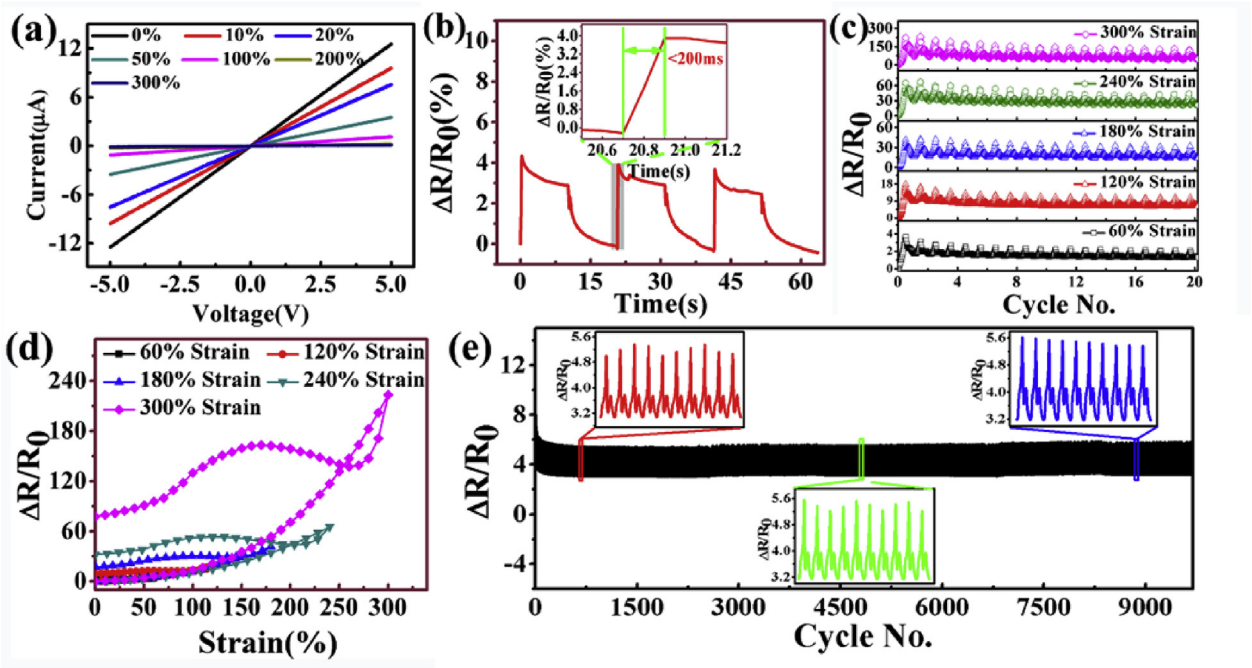

Fig. 4. (a) Current-voltage curves under different strains for MWCNTs/TPU composite strain sensor, (b) the response time of the strain sensor, (c) stretching-releasing cycles of the MWCNTs/TPU composite fiber under 60%, 120%, 180%, 240% and 300% strain, (d) the comparison of electrical responsive behaviors for the first cycle of (c). (e) The electrical response in 9700 cycles at a frequency of 0.05 Hz towards 0–100% strain. The insets in (e) show enlarged plots of 990–1000 cycles (red), 4990–5000 cycles (green) and 9000–9010 cycles (blue), respectively. (For interpretation of the references to colour in this figure legend, the reader is referred to the Web version of this article.)

maximum $\Delta R/R_0$ of the strain sensor increases as the strain loading rises. During the releasing process, a residual resistance is observed, which is ascribed to the viscoelastic feature of the TPU matrix [34]. Fig. 4d displays the relationship of $\Delta R/R_0$ in the first cycle towards the strain amplitudes of 60, 120, 180, 240 and 300%. It can be seen that the $\Delta R/R_0$ are hard to fully recover to the original state during the releasing process. Besides the effect of the viscoelasticity, this phenomenon is also related to the irreversible destruction of the conductive MWCNTs network, especially at a large strain [27]. Nevertheless, the sensing behaviors are stabilized gradually after several stretching-releasing cycles' treatment (Fig. 4c). The sensing stability and durability during more cycles are also evaluated. As shown in Fig. 4e, the composite fiber based strain sensor performs excellent stability during 9700 loading cycles (0.05 Hz under 100% strain) with a slight initial decline. Based on the results as mentioned above, good linearity, as well as wide response range, high sensitivity, rapid response time and good durability endows our fiber-shaped strain sensor with nice capability to monitor and recognize vigorous human activities.

3.3. Mechanism

As mentioned above, the $\Delta R/R_0$-strain curve is divided into two regions, showing two GFs of the strain sensor. The main reason for various areas is considered to be the evolution of MWCNTs conductive network aroused by the TPU matrix. Fig. 5 shows the change of $\Delta R/R_0$ as a function of strain for MWCNTs/TPU composite fibers. When the composite fibers are stretched blow 160% strain (area 1), the distance between neighboring MWCNTs is enlarged, and few connected points suffer damage [19]. Whereas due to the presence of the porous structure, the holes within the composite fibers are enlarged but still maintain a complete porous structure at this stage. The un-damaged hole walls as connected road for the conductive network make the conductive network remain relatively complete during the stretching. So a gentle resistance change is observed in composite fibers blow 160% strain. As further loading is applied, a rapid increase in $\Delta R/R_0$ is evidently observed above 160% strain (area 2). This different change can be related to the destruction of the hole walls, causing more breakage of conductive network at a higher strain. We explain the above phenomenon by using a mathematical model based on tunneling theory. Considering the previously reported literature [33], the total electrical resistance R of the composite can be defined with equation (1):

$$R = \left(\frac{L}{N}\right)\left(\frac{8\pi hs}{3\gamma a^2 e^2}\right)\exp(\gamma s) \tag{1}$$

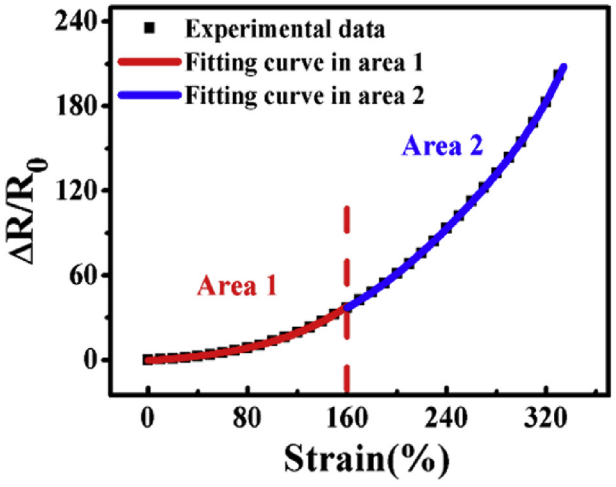

Fig. 5. The $\Delta R/R_0$-strain curves and fit curves for MWCNTs/TPU strain sensor.

Where N and L represent the number of conducting paths and particles forming a single conducting path, respectively, s is the smallest distance between adjacent conductive CNTs, h is the Plank constant, a^2 and e are the effective cross-section and the electron change, respectively. The γ is calculated by equation (2):

$$\gamma = \frac{4\pi}{h}\sqrt{2\phi m} \tag{2}$$

Where φ and m represent the height of the potential barrier between adjacent CNTs and the electron mass, respectively.

As a loading is applied, the particle separation and the number of conductive network will present a linear change and decrease versus the applied strain, respectively. For area 1 (the strain loading blow 160%), the hole and the hole walls within the composite fibers were enlarged and elongated, causing increasing distance between MWCNTs. Whereas the hole walls still maintain a connection during the period, so a gentle resistance change was observed. For area 2 of curve, a rapid increase in $\Delta R/R_0$ is evidently observed above 160% strain, which might be caused by the destruction of conductive network at a higher strain. It is also imaginable that the conductive pathways will decrease at a higher strain. Assuming that the separation between particles varies from s_0 to s, and the number of conductive network decreases from N_0 to N. It can be expressed as equations (3) and (4):

$$s = s_0(1 + m\varepsilon) \tag{3}$$

$$N = \begin{cases} \dfrac{N_0}{\exp(A_1\varepsilon + B_1)} & \varepsilon < 160\% \\ \dfrac{N_0}{\exp(A_2\varepsilon + B_2\varepsilon^2 + C\varepsilon^3 + D\varepsilon^4)} & \varepsilon \geq 160\% \end{cases} \tag{4}$$

where m is a constant, s_0 - initial particle separation, ε - the applied strain loading, N_0 - the number of conductive pathways in initial state, A_1, A_2, B_1, B_2, C and D are constants.

According to the above analysis, the relative resistance change $\Delta R/R_0$ is given by:

$$\frac{\Delta R}{R_0} = \frac{R - R_0}{R_0} = \left(\frac{N_0 S}{N S_0}\right)\exp[\gamma(s - s_0)] - 1 \tag{5}$$

Substitution of equations (3) and (4) into equation (5) yields:

$$\frac{\Delta R}{R_0} = \begin{cases} \{(1 + m_1\varepsilon)\exp(A\varepsilon + B_1) - 1 & \varepsilon < 160\% \\ (1 + m_2\varepsilon)\exp(A\varepsilon + B_2\varepsilon^2 + C\varepsilon^3 + D\varepsilon^4) - 1 & \varepsilon \geq 160\% \end{cases} \tag{6}$$

where $A = \begin{cases} A_1 + m_1\gamma s_0 & \varepsilon < 160\% \\ A_2 + m_2\gamma s_0 & \varepsilon \geq 160\% \end{cases}$. The outcome between experimental and fitting result corresponding to the area 1 and the area 2 was shown in Fig. 5. A high degree of consistency is achieved at $m = 0.07254$, $A = 0.00977$ and $B_1 = -0.43546$ for area 1. It can be also seen that the fitting curves resulting from equation (6) can depict the experimental data with $m = 0.29897$, $A = -0.02144$, $B_2 = 2.14408\times10^{-4}$, $C = -6.87004\times10^{-7}$, $D = 7.6899\times10^{-10}$ for area 2.

Hence, the tunneling conduction model can fit the experimental data in the full response range well (Fig. 5). It illustrates that the tunneling effect plays a predominant role in transporting charge carriers in the fiber-shaped strain sensor.

A schematic illustration and optical microscope images are displayed to better understand the strain sensing behavior (Fig. 6 and Fig. S9). Fig. 6a shows that the porous structure (red ellipse) in the MWCNTs/TPU composite fibers, MWCNTs disperse randomly in the hole walls and other solid parts, forming a compact conductive network. When the composite fibers are stretched (blow 160% strain) (Fig. 6b), due to the mechanical flexibility of MWCNTs, they stretch and wriggle with the TPU matrix, resulting in the increase of the tunneling distance between MWCNTs (blue circle) and the breakage of few conductive pathways. However, a relatively complete conductive network

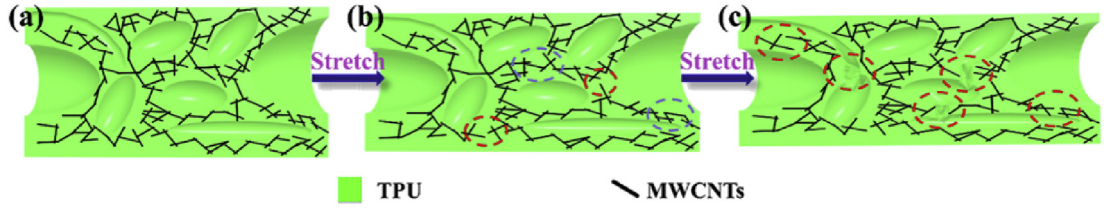

Fig. 6. Schematic illustration for the evolution of the conductive network during the stretching process. (a) The initial state; (b) the stretching state lower than 160% strain; (c) the stretching state upon 160% strain.

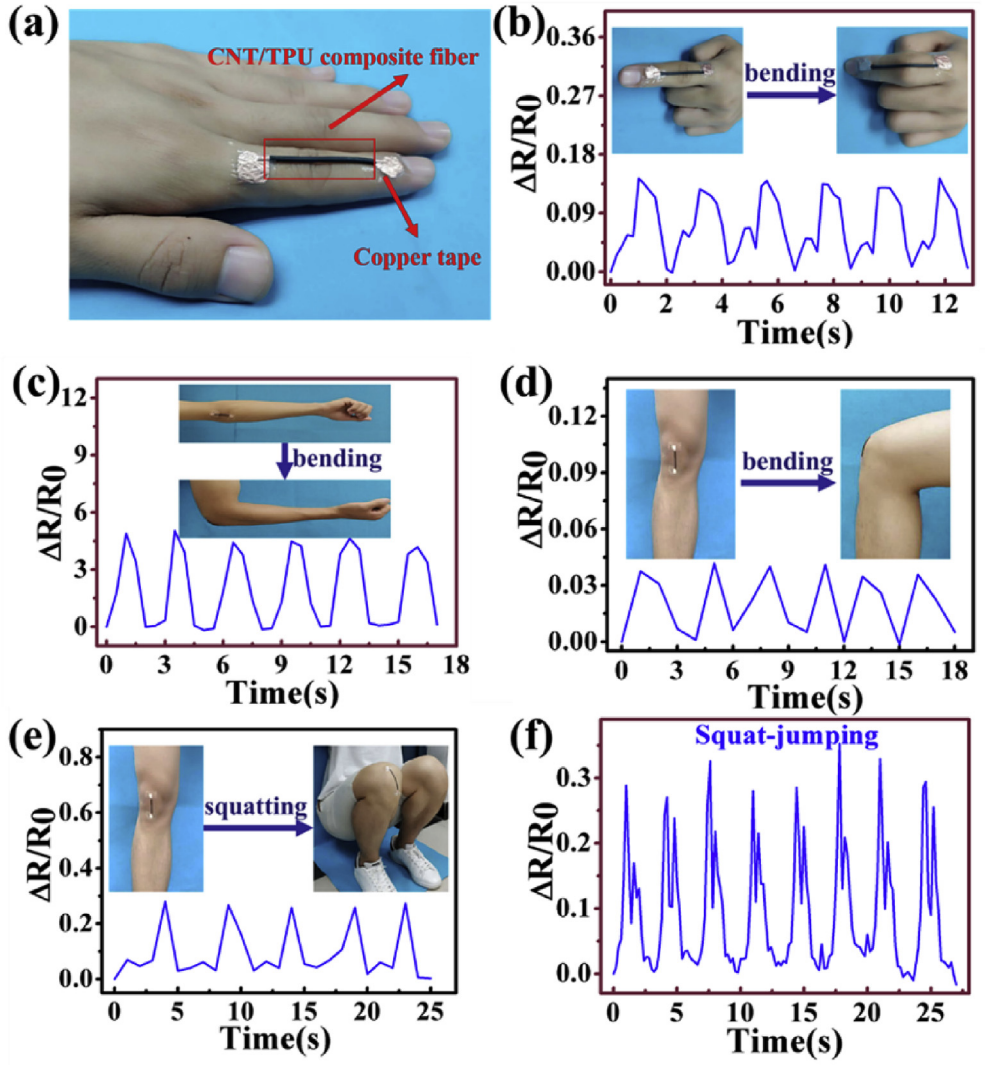

Fig. 7. The application in human motions for strain sensor. (a) Digital photo of strain sensor attached onto finger with the assistance of medical water proof PU membranes. The response behavior of (b) finger bending, (c) elbow bending, (d) knee bending, (e) squatting and (f) squat-jumping. The inset digital photos show the human motions.

is maintained, which is owing to the un-damaged hole walls. And a gentle increasing of the resistance is observed during this period. With further stretching (above 160% strain), more breakage of conductive pathways and crack of the hole walls (red ellipse) appears (Fig. 6c and Fig. S9), resulting in the rapid increase of the resistance, which performs as a high GF. Therefore, owing to the breakage of conductive pathways and the enlarged distance between MWCNTs, the responsivity increases sharply as shown in Figs. 3a and 5.

3.4. Human motion monitoring

The high sensitive, board response range, rapid response time, durability and excellent flexibility enable our MWCNTs/TPU fiber to be well used in wearable devices to monitor various human motions. The as-prepared strain sensor is then pasted onto different joints of human body by using medical water proof PU membranes (Fig. 7a), which is used to insulate the human body and the strain sensor to eliminate the

effect of human resistance on the sample in the corresponding process. Fig. 7b shows that the strain sensor is attached onto the finger to monitor the real-time motions. The $\Delta R/R_0$ increases along with the bending of the finger, and decreases as the finger returns to the straightened state. It exhibits an excellent and stable electrical response to the motions of the finger.

Similar to the finger, the elbow bending (Fig. 7c) and the knee bending (Fig. 7d) display a rapid and repeatable response behavior and a different sensitivity. The interesting consequence is attributed to the different amplitude at various joint during exercising. Moreover, the strain sensor is sensitive to detect different motions by distinguishing the various peak shapes of curves. As observed in Fig. 7e, the strain sensor illustrates a single peak during the squatting process. For squatting-jumping, as shown in Fig. 7f, two peaks would be recorded because the action consists of two motions (squatting and jumping). The first peak and second peak correspond to the motion of squatting and jumping, respectively, showing a high resolution. In a word, the results demonstrate that our strain sensor can be applied as a nice candidate in smart wearable devices.

4. Conclusion

In summary, we fabricated a MWCNTs/TPU composite fiber based wearable strain sensor with an interesting porous structure. The fiber-shaped strain sensors showed wide response range (320%) and high sensitivity (GF of 22.2 within 160% strain and 97.1 for a strain of 160–320%). The strain sensor also displayed a fast response time (< 200 ms). The electrical response for the MWCNTs/TPU strain sensor was very steady even in 9700 cycles at a large strain of 100%, showing superior reproducibility and excellent durability. The mechanism of the evolution of the conductive network under tension test was studied through the tunneling theory. The applications of strain sensor based on MWCNTs/TPU composite fibers in monitoring human activities including vigorous motions such as bending of the fingers, elbows and knee, squatting and squat-jumping were demonstrated. This work provides a good strategy to fabricate high performance fiber-shaped strain sensor with wide response range and high sensitivity for human motion monitoring.

Acknowledgments

The authors gratefully acknowledge the financial support of this work by the National Natural Science Foundation of China (contract number 51603193, 51773183, 11572290, 11432003), the National Natural Science Foundation of China-Henan Province Joint Funds (contract number U1604253).

Appendix A. Supplementary data

Supplementary data to this article can be found online at https://doi.org/10.1016/j.compscitech.2018.09.006.

References

[1] H. Wu, Q. Liu, W. Du, C. Li, G. Shi, Transparent polymeric strain sensors for monitoring vital signs and beyond, ACS Appl. Mater. Interfaces 10 (4) (2018) 3895–3901.
[2] S. Nag-Chowdhury, H. Bellegou, I. Pillin, M. Castro, P. Longrais, J.F. Feller, Non-intrusive health monitoring of infused composites with embedded carbon quantum piezo-resistive sensors, Compos. Sci. Technol. 123 (2016) 286–294.
[3] Y. He, Q. Gui, Y. Wang, Z. Wang, S. Liao, Y. Wang, A polypyrrole elastomer based on confined polymerization in a host polymer network for highly stretchable temperature and strain sensors, Small 14 (19) (2018) 1800394.
[4] Y. Yu, Y. Luo, A. Guo, L. Yan, Y. Wu, K. Jiang, Q. Li, S. Fan, J. Wang, Flexible and transparent strain sensors based on super-aligned carbon nanotube films, Nanoscale 9 (20) (2017) 6716–6723.
[5] X. Shi, S. Liu, Y. Sun, J. Liang, Y. Chen, Lowering internal friction of 0d-1d-2d ternary nanocomposite-based strain sensor by fullerene to boost the sensing performance, Adv. Funct. Mater. 28 (22) (2018) 1800850.
[6] M. Zhang, C. Wang, H. Wang, M. Jian, X. Hao, Y. Zhang, Carbonized cotton fabric for high-performance wearable strain sensors, Adv. Funct. Mater. 27 (2) (2017) 1604795.
[7] Y. Zheng, Y. Li, K. Dai, Y. Wang, G. Zheng, C. Liu, C. Shen, A highly stretchable and stable strain sensor based on hybrid carbon nanofillers/polydimethylsiloxane conductive composites for large human motions monitoring, Compos. Sci. Technol. 156 (2018) 276–286.
[8] S. Liu, Y. Lin, Y. Wei, S. Chen, J. Zhu, L. Liu, A high performance self-healing strain sensor with synergetic networks of poly(3-caprolactone) microspheres, graphene and silver nanowires, Compos. Sci. Technol. 146 (2017) 110–118.
[9] S. Gong, D.T.H. Lai, B. Su, K.J. Si, Z. Ma, L.W. Yap, P. Guo, W. Cheng, Highly stretchy black gold e-skin nanopatches as highly sensitive wearable biomedical sensors, Adv. Electron. Mater. 1 (4) (2015) 1400063.
[10] S. Gong, D.T. Lai, Y. Wang, L.W. Yap, K.J. Si, Q. Shi, N.N. Jason, T. Sridhar, H. Uddin, W. Cheng, Tattoolike polyaniline microparticle-doped gold nanowire patches as highly durable wearable sensors, ACS Appl. Mater. Interfaces 7 (35) (2015) 19700–19708.
[11] S. Chen, Y. Wei, X. Yuan, Y. Lin, L. Liu, A highly stretchable strain sensor based on a graphene/silver nanoparticle synergic conductive network and a sandwich structure, J. Mater. Chem. C 4 (19) (2016) 4304–4311.
[12] X. Wu, Y. Han, X. Zhang, C. Lu, Highly sensitive, stretchable, and wash-durable strain sensor based on ultrathin conductive layer@polyurethane yarn for tiny motion monitoring, ACS Appl. Mater. Interfaces 8 (15) (2016) 9936–9945.
[13] M.D. Ho, Y. Ling, L.W. Yap, Y. Wang, D. Dong, Y. Zhao, W. Cheng, Percolating network of ultrathin gold nanowires and silver nanowires toward “invisible” wearable sensors for detecting emotional expression and apexcardiogram, Adv. Funct. Mater. 27 (25) (2017) 1700845.
[14] L. Ma, W. Yang, Y. Wang, H. Chen, Y. Xing, J. Wang, Multi-dimensional strain sensor based on carbon nanotube film with aligned conductive networks, Compos. Sci. Technol. 165 (2018) 190–197.
[15] T. Li, J.-H. Pu, L.-F. Ma, R.-Y. Bao, G.-Q. Qi, W. Yang, B.-H. Xie, M.-B. Yang, An extremely uniform dispersion of MWCNTs in olefin block copolymers significantly enhances electrical and mechanical performances, Polym. Chem. 6 (40) (2015) 7160–7170.
[16] M. Hempel, D. Nezich, J. Kong, M. Hofmann, A novel class of strain gauges based on layered percolative films of 2D materials, Nano Lett. 12 (11) (2012) 5714–5718.
[17] X. Wang, Y. Qiu, W. Cao, P. Hu, Highly stretchable and conductive core-sheath chemical vapor deposition graphene fibers and their applications in safe strain sensors, Chem. Mater. 27 (20) (2015) 6969–6975.
[18] Y. Cheng, R. Wang, J. Sun, L. Gao, A stretchable and highly sensitive graphene-based fiber for sensing tensile strain, bending, and torsion, Adv. Mater. 27 (45) (2015) 7365–7371.
[19] Y. Zheng, Y. Li, Z. Li, Y. Wang, K. Dai, G. Zheng, C. Liu, C. Shen, The effect of filler dimensionality on the electromechanical performance of polydimethylsiloxane based conductive nanocomposites for flexible strain sensors, Compos. Sci. Technol. 139 (2017) 64–73.
[20] C. Wang, K. Xia, M. Jian, H. Wang, M. Zhang, Y. Zhang, Carbonized silk georgette as an ultrasensitive wearable strain sensor for full-range human activity monitoring, J. Mater. Chem. C 5 (30) (2017) 7604–7611.
[21] R. Moriche, A. Jimenez-Suarez, M. Sanchez, S.G. Prolongo, A. Urena, Graphene nanoplatelets coated glass fibre fabrics as strain sensors, Compos. Sci. Technol. 146 (2017) 59–64.
[22] Z. Wang, Y. Huang, J. Sun, Y. Huang, H. Hu, R. Jiang, W. Gai, G. Li, C. Zhi, Polyurethane/cotton/carbon nanotubes core-spun yarn as high reliability stretchable strain sensor for human motion detection, ACS Appl. Mater. Interfaces 8 (37) (2016) 24837–24843.
[23] L. Li, P. Shi, L. Hua, J. An, Y. Gong, R. Chen, C. Yu, W. Hua, F. Xiu, J. Zhou, G. Gao, Z. Jin, G. Sun, W. Huang, Design of a wearable and shape-memory fibriform sensor for the detection of multimodal deformation, Nanoscale 10 (1) (2017) 118–123.
[24] M. Ji, H. Deng, D. Yan, X. Li, L. Duan, Q. Fu, Selective localization of multi-walled carbon nanotubes in thermoplastic elastomer blends: an effective method for tunable resistivity-strain sensing behavior, Compos. Sci. Technol. 92 (2014) 16–26.
[25] Y. Wang, J. Hao, Z. Huang, G. Zheng, K. Dai, C. Liu, C. Shen, Flexible electrically resistive-type strain sensors based on reduced graphene oxide-decorated electrospun polymer fibrous mats for human motion monitoring, Carbon 126 (2018) 360–371.
[26] J.H. Pu, X.J. Zha, M. Zhao, S. Li, R.Y. Bao, Z.Y. Liu, B.H. Xie, M.B. Yang, Z. Guo, W. Yang, 2D end-to-end carbon nanotube conductive networks in polymer nanocomposites: a conceptual design to dramatically enhance the sensitivities of strain sensors, Nanoscale 10 (5) (2018) 2191–2198.
[27] Y. Lu, J. Jiang, S. Yoon, K.S. Kim, J.H. Kim, S. Park, S.H. Kim, L. Piao, High-performance stretchable conductive composite fibers from surface-modified silver nanowires and thermoplastic polyurethane by wet spinning, ACS Appl. Mater. Interfaces 10 (2) (2018) 2093–2104.
[28] Z. Jia, C. Lu, Y. Liu, P. Zhou, L. Wang, Lignin/polyacrylonitrile composite hollow fibers prepared by wet-spinning method, ACS Sustain. Chem. Eng. 4 (5) (2016) 2838–2842.
[29] P. Sukitpaneenit, T.-S. Chung, Molecular elucidation of morphology and mechanical properties of PVDF hollow fiber membranes from aspects of phase inversion, crystallization and rheology, J. Membr. Sci. 340 (1–2) (2009) 192–205.
[30] M.R. Thompson, G.H. Motlagh, K.J. Oxby, A.N. Hrymak, Multiple percolation in a carbon-filled polymer composites via foaming, J. Appl. Polym. Sci. 115 (2) (2010) 646–654.
[31] G.H. Motlagh, A.N. Hrymak, M.R. Thompson, Improved through-plane electrical conductivity in a carbon-filled thermoplastic via foaming, Polym. Eng. Sci. 48 (4) (2008) 687–696.
[32] L. Duan, S. Fu, H. Deng, Q. Zhang, K. Wang, F. Chen, Q. Fu, The resistivity-strain behavior of conductive polymer composites: stability and sensitivity, J. Mater. Chem. A 2 (40) (2014) 17085–17098.
[33] Y. Lin, S. Liu, S. Chen, Y. Wei, X. Dong, L. Liu, A highly stretchable and sensitive strain sensor based on graphene-elastomer composites with a novel double-interconnected network, J. Mater. Chem. C 4 (26) (2016) 6345–6352.
[34] H. Liu, J. Gao, W. Huang, K. Dai, G. Zheng, C. Liu, C. Shen, X. Yan, J. Guo, Z. Guo, Electrically conductive strain sensing polyurethane nanocomposites with synergistic carbon nanotubes and graphene bifillers, Nanoscale 8 (26) (2016) 12977–12989.